Transverse Resonance, Standing Wave, and Resonator Formulations of the Ridge Waveguide Eigenvalue Problem and Its Application to the Design of E-Plane Finned Waveguide Filters

JENS BORNEMANN, MEMBER, IEEE, AND FRITZ ARNDT, SENIOR MEMBER, IEEE

Abstract—**Utilizing the rigorous field distribution of the ridge waveguide eigenmodes, this paper presents an accurate computer-aided design of compact, low-cost, low-insertion-loss evanescent-mode waveguide band-pass filters with bilateral metallic E-plane fins. The design theory takes into account the influences of both the finite fin thickness and the higher order mode interaction at all discontinuities. The numerical advantage of the transverse resonance method for solving the related cross-sectional eigenvalue problem is demonstrated for the design of quasi-high-pass and band-pass filters of different ridge gap widths and is compared with the classical standing wave and resonator mode-matching techniques. Computer-optimized design data are given for filters with passbands in X-band (8–12 GHz) and E-band (60–90 GHz), which achieve high skirt selectivity and wide stopband. The theory is verified by measurements.**

I. Introduction

RIDGED and finned waveguide circuits have found many applications in microwave and millimeter wave devices [1]–[15]. The advantages of these circuits include large single-mode broad-band operation and, in its finned version with thin ridges, the possibility of low-cost, low-loss E-plane integrated circuit designs. Various field-theory approaches have been reported for the characterization of the ridge waveguide discontinuity [7], [8], [12]–[14]. Most of the techniques presented are either based on approximate equations for the field distribution in ridge waveguides or neglect the influence of the finite metallization thickness. However, the effects of both the accurate field description of the ridge waveguide sections and the metallization thickness have turned out to be important for reliable filter designs with cascaded all-metal finline discontinuities.

Bilateral or unilateral ridge waveguide sections are often used to construct distributed shunt capacitances in low-pass filter designs [11], [15]. More recently, nontouching unilateral E-plane fins of negligible thickness with and without a dielectric layer [12] have been applied for the design of evanescent-mode band-pass filters. Such filters [12], [16]–[18] are of particular importance due to several advantages over the conventional filter types, e.g. compactness and wide stopbands. The usual thick ridge waveguide, capacitive screw, and round post filter elements, however, are often difficult to fabricate at low cost and to mass-produce [15]–[18]. On the other hand dielectric layers cause additional losses; hence the low-insertion-loss design potential inherent in the finned waveguide technology may not be fully utilized. Moreover thin unilateral fins may lead to small ridge gaps, and therefore may achieve a low power handling capability [12].

In this paper, a rigorous field theory description of the ridge waveguide is utilized to formulate the modal scattering matrix of the waveguide-to-ridge-waveguide discontinuity, which is the basic building block in the design. The computed response, however, is extremely sensitive to different cross-section eigenfunction formulations, because the separation constants and normalization factors involved have to be numerically calculated before the matching procedure in the propagation direction. These quantities directly influence the complexity, the numerical accuracy with respect to the number of expansion terms considered, and the computational effort for the three-dimensional mode-matching process.

Therefore special emphasis is placed on the selection of a stable and reliable design method. Three distinct mode-matching techniques, each having its individual advantages, are applied to solve the special eigenvalue problem for the purpose of investigating their suitability for the efficient analysis of finned waveguide discontinuities. The first is the transverse resonance method, which has turned out to be well suited to dealing with complicated waveguide sections [13], [19]–[21]; the second is the conventional standing wave method [22], which shows the advantage of independent numbers of expansion functions in the subregions; and the third is the resonator

Manuscript received March 30, 1989; revised February 27, 1990.

J. Bornemann is with the Department of Electrical and Computer Engineering, University of Victoria, P.O. Box 1700, Victoria, B.C., V8W2Y2 Canada.

F. Arndt is with the Microwave Department, University of Bremen, Kufsteiner Str., NW1, D-2800 Bremen, West Germany.

IEEE Log Number 9036423.

0018-9480/90/0800-1104$01.00

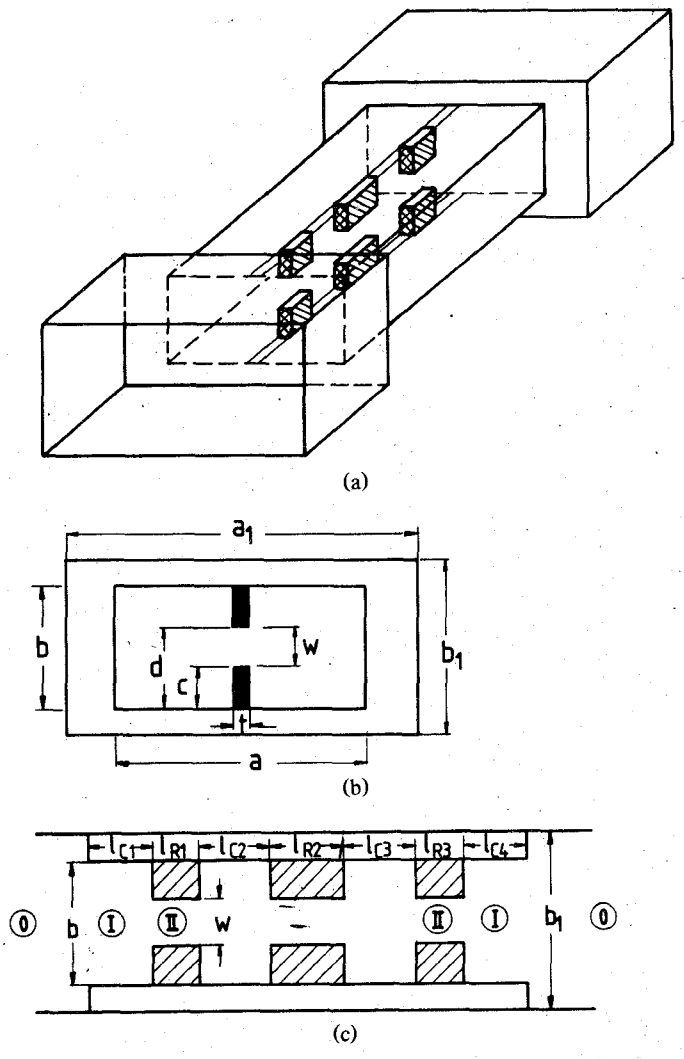

Fig. 1. Evanescent-mode bilateral E-plane finned waveguide band-pass filter. (a) Input and output waveguide, below-cutoff waveguide with E-plane fins of thickness t. (b) Cross-sectional dimensions. (c) Longitudinal section dimensions in the filter region.

method, which is reported to yield a more appropriate numerical procedure [23]. In contrast to [22] and [23], in this paper all three techniques are based on a six-component representation of the electromagnetic field and on the inclusion of TM- to- TE-mode coupling effects.

The rigorous modal scattering matrix description of ridge waveguide discontinuities is then applied to provide an efficient computer-aided design method for a type of millimeter-wave printed circuit evanescent-mode waveguide band-pass filter (Fig. 1). Based on bilateral all-metal E-plane fins, the design combines the well-known properties of the waveguide E-plane integrated-circuit technology [7], [11], [12] with the advantages of the evanescent-mode concept [15]–[18] and the low-insertion-loss quality resulting from the complete absence of supporting dielectrics [24]. The proposed structure, where the finite fin thickness is included in the design, achieves relatively large gap widths (about one quarter of the waveguide height in the below-cutoff section) and leads to filter characteristics with high skirt selectivity and wide stopbands. Moreover, the exact design theory presented permits high-precision manufacturing by etching or milling techniques without the necessity of postassembly trial and error adjustment methods.

The immediate modal S-matrix combination of all interacting structures includes the higher order mode coupling effects and allows the stopband characteristics of the filters to be taken into account for the filter design. For computer optimization, the evolution strategy method [13], [24], i.e., a suitably modified direct search procedure, is applied where no differentiation step in the optimization process is necessary; hence the problem of local minima may be circumvented. Design examples for optimized evanescent-mode E-plane finned band-pass filters with passbands at about 11 GHz and 75 GHz are given. The design for 11 GHz uses WR 90 waveguides above cutoff for the input and output sections and a WR 42 waveguide below cutoff for the filter section. For the 75 GHz design example, WR 12 waveguides above cutoff and a WR 7 waveguide below cutoff, reduced in height, are applied. The filters achieve high attenuation over a wide second stopband. The theory is verified by measured results of an E-plane finned WR 62 structure and a WR 90 evanescent-mode filter.

II. Theory

A. Field Description with Two Vector Potential Components

For the computer-aided design of the evanescent-mode E-plane finned waveguide filter (Fig. 1), the modal S-matrix method [13], [19], [20], [24] is applied. The filter structure is decomposed into two key building block discontinuities: the double step junction from the input waveguide above-cutoff to the waveguide below-cutoff filter section, and the step discontinuity from the rectangular waveguide to the E-plane finned waveguide. Note that for the corresponding inverse structure (e.g., the junction from waveguide below cutoff to waveguide above cutoff), the related modal scattering matrix is simply derived by interchanging the corresponding submatrix elements of the original structure. Combination with the known scattering matrices of the corresponding intermediate homogeneous waveguide sections of finite lengths yields the total scattering matrix of the filter.

Since a rigorous field description of the step discontinuities involved (Fig. 1) requires all field components as well as the TM-to-TE coupling effects to be considered, the electromagnetic field in the subregions $i = 0$, I, II (Fig. 1(c)),

$$\vec{E}^i = \nabla \times \left(A^i_{Hz}\vec{e}_z\right) + \frac{1}{j\omega\epsilon}\nabla \times \nabla \times \left(A^i_{Ez}\vec{e}_z\right)$$

$$\vec{H}^i = \nabla \times \left(A^i_{Ez}\vec{e}_z\right) - \frac{1}{j\omega\mu}\nabla \times \nabla \times \left(A^i_{Hz}\vec{e}_z\right) \qquad (1)$$

is derived from the z components of two vector poten-

tials,

$$\vec{A}^i_{Hz} = \sum_{q=1}^{\infty} \left(\sqrt{Z^i_{Hq}}\right) \cdot T^i_{Hq}(x,y) \cdot \left[V^i_{Hq} \exp\left(-jk^i_{zHq} z\right) + R^i_{Hq} \exp\left(+jk_{zHq} z\right)\right]$$

$$\vec{A}^i_{Ez} = \sum_{p=1}^{\infty} \left(\sqrt{Y^i_{Ep}}\right) \cdot T^i_{Ep}(x,y) \cdot \left[V^i_{Ep} \exp\left(-jk^i_{zEp} z\right) - R^i_{Ep} \exp\left(+jk_{zEp} z\right)\right] \quad (2)$$

with the wave impedances

$$Z^i_{Hq} = (\omega\mu_0)/\left(k^i_{zHq}\right) = 1/Y^i_{Hq}$$
$$Y^i_{Ep} = (\omega\epsilon_0)/\left(k^i_{zEp}\right) = 1/Z^i_{Ep}. \quad (3)$$

V^i_H, E and $R^i_{H,E}$ are the TE- and TM-mode wave amplitudes of the forward and backward waves, respectively, which have to be related to each other at the corresponding discontinuity. This will yield the corresponding scattering matrix relations. The propagation factors are denoted by k_z, and T^i_{Hq}, T^i_{Ep} are the cross-section eigenfunctions of the corresponding waveguide structures under consideration. For the rectangular waveguide sections (regions $i = 0, \mathrm{I}$), the relations of [25] are given for completeness, using the present notation:

1) Input–output waveguide (region 0):

$$T^0_{Hq}(x,y) = A^0_q \cos\left[(2m-1)\frac{\pi}{a_1}x\right] \cdot \left(\cos\frac{2n\pi}{b_1}y\right)/\left(\sqrt{1+\delta_{0n}}\right)$$
$$T^0_{Ep}(x,y) = D^0_p \sin\left[(2m-1)\frac{\pi}{a_1}x\right] \cdot \sin\frac{2n\pi}{b_1}y. \quad (4)$$

2) Waveguide below cutoff (region I):

$$T^{\mathrm{I}}_{Hq}(x,y) = A^{\mathrm{I}}_q \cos\left[(2m-1)\frac{\pi}{a}x\right] \cdot \left(\cos\frac{2n\pi}{b}y\right)/\left(\sqrt{1+\delta_{0n}}\right)$$
$$T^{\mathrm{I}}_{Ep}(x,y) = D^{\mathrm{I}}_p \sin\left[(2m-1)\frac{\pi}{a}x\right] \cdot \sin\frac{2n\pi}{b}y. \quad (5)$$

For the E-plane finned or ridged waveguide eigenvalue problem (region II), the transverse resonance, the standing wave, and the resonator method are used and compared with each other.

B. E-Plane Finned or Ridged Waveguide Eigenvalue Problem

Three different mode-matching methods are investigated to solve rigorously the cross-sectional boundary value problem of the finned or ridged waveguide (Fig. 2). As the formulations directly influence the solution of the related discontinuity problem with regard to complexity, the computational effort, and the numerical accuracy in relation to the expansion terms considered, a comparison of these three rigorous standard field theory methods is particularly indicated. The functions T^{II}_{Hq} and T^{II}_{Ep} may conveniently be simplified utilizing the magnetic wall and electric wall symmetries at $x = a/2$ and $y = b/2$, respectively.

1) Transverse Resonance Method (TRM): By considering propagation to take place in the x direction, an inhomogeneous waveguide cross section can be regarded as a transmission line subdivided into homogeneous subregions [13], [19]–[21]. A transverse transmission-line matrix relates the field amplitudes at the lower and the upper boundary of each subregion. Finally, the line resonator resonance condition is satisfied by the thus far neglected boundary condition at the metallic sidewalls. For the ridge or finned waveguide cross section under consideration (Fig. 2(a)), the transverse resonance method with the boundary conditions to be applied in the x direction (in our case electric wall at $x = 0$, magnetic wall at $x = a/2$) provides the corresponding homogeneous system of equations, requiring the system determinant to be zero [13], [19]–[21].

The cross-section eigenfunctions are expressed in terms of the x- and y-dependent functions of subregions IIa and IIb:

$$T^{\mathrm{II}}_{Hq}(x,y) = \sum_{n=}^{N} \left[A^{\mathrm{IIa}}_{qn}\left(1/k^{\mathrm{IIa}}_{xHqn}\right) \sin\left(k^{\mathrm{IIa}}_{xHqn}\left(x - \frac{a}{2}\right)\right) \cdot \left(\cos\left(\frac{n\pi}{\frac{b}{2}-c}(y-c)\right)\right)/\left(\sqrt{1+\delta_{0n}}\right) + A^{\mathrm{IIb}}_{qn} \cos\left(k^{\mathrm{IIb}}_{xHqn}x\right)\left(\cos\frac{2n\pi}{b}y\right)/\left(\sqrt{1+\delta_{0n}}\right)\right]$$

$$T^{\mathrm{II}}_{Ep}(x,y) = \sum_{n=1}^{N} \left[D^{\mathrm{IIa}}_{pn} \cos\left(k^{\mathrm{IIa}}_{xEpn}\left(x - \frac{a}{2}\right)\right) \cdot \sin\left(\frac{n\pi}{\frac{b}{2}-c}(y-c)\right) + D^{\mathrm{IIb}}_{pn}\left(1/k^{\mathrm{IIb}}_{xEpn}\right) \sin\left(k^{\mathrm{IIb}}_{xEpn}x\right) \sin\left(\frac{2n\pi}{b}y\right)\right] \quad (6)$$

where superscripts IIa and IIb denote, respectively, the corresponding terms in the finned waveguide sub–cross sections (Fig. 2(a)), and the k_x's are calculated by solving the related cross-section eigenvalue problem [13].

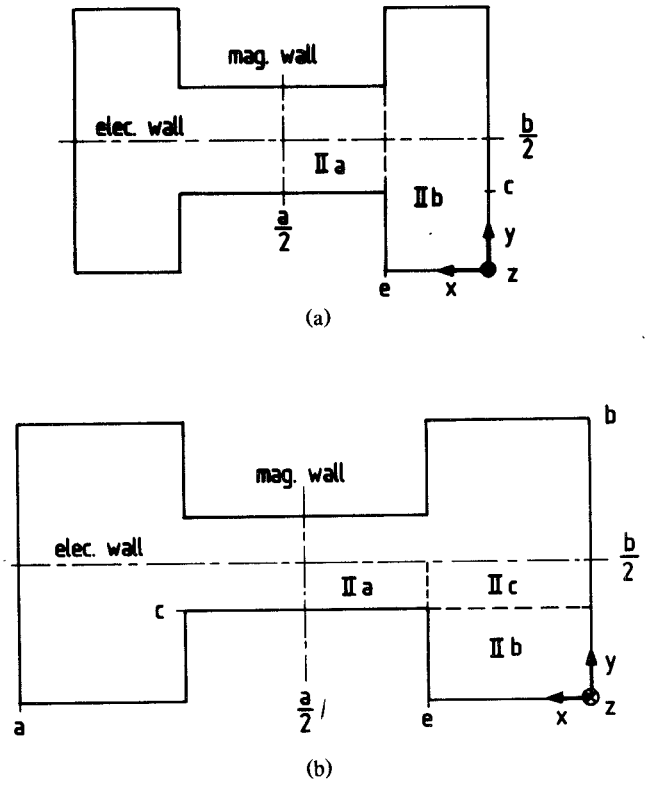

Fig. 2. Finned or ridged waveguide cross section. (a) Subregions for the transverse resonance method (TRM) and the standing wave formulation (SWF). (b) Subregions for the resonator method (RM).

The transverse resonance procedure reduces the size of the characteristic matrix equation to a quarter of the original size. Furthermore, it makes the method very flexible because an arbitrary number of subregions (e.g. finlines with multiple inserts [20]) may be easily taken into account in the matrix system simply by multiplying the additional transmission-line matrices of the corresponding insert subregions. On the other hand, due to the transverse resonance technique [13], the number N of the expansion terms must be the same for both subregions. For very small slot widths of about $w/b < 0.1$ (cf. Fig. 1(b)), therefore, the related limited number of expansion terms in this case may lead to a poor convergence behavior.

However, the main advantage of the transverse resonance method described is the fact that there are no poles in the determinant function of the resulting characteristic matrix equation. Therefore the search algorithm to find a given number of subsequent eigenvalues (i.e. the propagation constants for a given frequency, or, as in the present case, the cutoff frequencies) can be simplified and the risk of omitting eigenvalues is very low, in contrast to both other methods under consideration.

2) Standing Wave Formulation (SWF): For this formulation, the tangential field components E_y, H_z or E_z, H_y are matched directly at the common interface at $x = e$ (cf. Fig. 2(a)), which results in two homogeneous matrix equations [22]. Assuming that the numbers M and N correspond to subregions IIa and IIb (Fig. 2(a)), respectively, with $M < N$, then the cross-section eigenfunctions are given by

$$T_{Hq}^{\mathrm{II}}(x,y) = \sum_{m=}^{M} A_{qm}^{\mathrm{IIa}}\left(1/k_{xHqm}^{\mathrm{IIa}}\right)\sin\left(k_{xHqm}^{\mathrm{IIa}}\left(x-\frac{a}{2}\right)\right)$$
$$\cdot\left(\cos\left(\frac{m\pi}{\frac{b}{2}-c}(y-c)\right)\right)/\left(\sqrt{1+\delta_{0m}}\right)$$
$$+\sum_{n=0}^{N} A_{qn}^{\mathrm{IIb}}\cos\left(k_{xHqn}^{\mathrm{IIb}}x\right)$$
$$\cdot\left(\cos\frac{2n\pi}{b}y\right)/\left(\sqrt{1+\delta_{0n}}\right)\Bigg]$$

$$T_{Ep}^{\mathrm{II}}(x,y) = \sum_{m=1}^{M} D_{pm}^{\mathrm{IIa}}\cos\left(k_{xEpm}^{\mathrm{IIa}}\left(x-\frac{a}{2}\right)\right)$$
$$\cdot\sin\left(\frac{m\pi}{\frac{b}{2}-c}(y-c)\right)$$
$$+\sum_{n=1}^{N} D_{pn}^{\mathrm{IIb}}\left(1/k_{xEpn}^{\mathrm{IIb}}\right)$$
$$\cdot\sin\left(k_{xEpn}^{\mathrm{IIb}}x\right)\sin\left(\frac{2n\pi}{b}y\right).$$

This expression is essentially equivalent to that given in (6), but with the notable exception that the numbers M and N of the expansion terms may be independently chosen in each subregion. This advantage, however, is undermined by the fact that, particularly for higher order modes, the determinant function of the characteristic matrix equation yields zeros with poles in the immediate vicinity. As a consequence, certain eigenvalues of higher order modes, which can have a significant influence on the three-dimensional field distribution (especially for small gap widths), may not be detected, and the resulting modal scattering matrix parameters are no longer fully reliable.

3) Resonator Method (RM): In order to apply the resonator method [23], the cross section (Fig. 2(b)) has to be divided into three subregions, one of which is called the resonator region: IIc. The basic idea of this approach is to force the electric field to be zero at $x = e$ and $y \in (0, c)$ in contrast to the two preceding methods, where this condition is met indirectly by adding up a number of expansion terms. Therefore the propagation is considered to take place in the y direction for region IIb. By applying the superposition principle and matching the fields of subregions IIb to IIc at $y = c$, and those of IIa to IIc at $x = e$, the resonator functions (IIc) can be expressed in terms of the subregions IIa and IIb, respectively [23].

As a result, the cross-section eigenfunctions read

$$T_{Hq}^{\mathrm{II}}(x,y) = \sum_{m=0}^{M} A_{qm}^{\mathrm{IIa}} F_{xHqm}^{\mathrm{IIa}} \left(\cos\left(\frac{m\pi}{\frac{b}{2}-c}(y-c) \right) \right) \Big/ \left(\sqrt{1+\delta_{0m}} \right) + \sum_{n=0}^{N} A_{qn}^{\mathrm{IIb}} F_{yHqn}^{\mathrm{IIb}} \left(\cos \frac{n\pi}{e} x \right) \Big/ \left(\sqrt{1+\delta_{0n}} \right)$$

$$T_{Ep}^{\mathrm{II}}(x,y) = \sum_{m=1}^{M} D_{pm}^{\mathrm{IIa}} F_{xEpm}^{\mathrm{IIa}} \sin\left(\frac{m\pi}{\frac{b}{2}-c}(y-c) \right) + \sum_{n=1}^{N} D_{pn}^{\mathrm{IIb}} F_{yxEpn}^{\mathrm{IIb}} \sin\left(\frac{n\pi}{e} x \right) \tag{8}$$

where the expressions F_x and F_y are elucidated in the Appendix.

The more complicated structure of these functions, compared with (6) and (7), is caused by the additional plane of subregion interaction due to the division into three subsections (Fig. 2(b)). At first glance, the resonator method seems to be a very attractive technique for solving this eigenvalue problem, as it combines the advantage of the independent choice of the number of expansion terms in subregions IIa and IIb with the feature that the boundary condition at the plane $x=e$, $y \in (0,c)$ is exactly satisfied by the corresponding resonator function, which does not depend on the number of expansion terms considered. However, the situation associated with the determinant function of the related characteristic matrix equation has turned out to be still more severe than that of the standing wave formulation: the poles in the immediate vicinity of the zeros to be detected require a very time consuming search algorithm. Despite this effort, eigenvalues may be overlooked which would otherwise have been found relatively easily with the transverse resonance method.

C. Modal Scattering Matrix

In order to calculate the modal scattering matrix of the key building block discontinuities of the filter component (Fig. 1), the coefficients A_q^0, D_p^0, A_q^{I}, and D_p^{I} in (4) and (5) and the amplitude vectors of the expansion functions A_q^{IIa}, A_q^{IIb}, D_p^{IIa}, and D_p^{IIb} in (6)–(8) are normalized so that the power carried by a given mode is

$$P_M^{\iota} = \int_{F^{\iota}} \left(\vec{E}_M^{\iota} \times \vec{H}_M^{\iota} \right) \vec{e}_z \, dF = \sqrt{Z_M^{\iota}} \sqrt{Y_M^{\iota}} \int_{F^{\iota}} \left(\operatorname{grad} T_M^{\iota} \right)^2 dF = \begin{cases} 1\ \mathrm{W}, & \text{propagating modes} \\ j\ \mathrm{W}, & \text{evanescent modes} \\ -j\ \mathrm{W}, & \text{evanescent TM modes.} \end{cases} \tag{9}$$

In this equation, the subscript M replaces the indices Hq and Ep for TE and TM modes, respectively. Matching the tangential field components of regions I and II at the common interface yields the modal scattering matrix (S) of the related discontinuity waveguide to finned waveguide:

$$\begin{bmatrix} (R^{\mathrm{I}}) \\ (V^{\mathrm{II}}) \end{bmatrix} = (S) \begin{bmatrix} (V^{\mathrm{I}}) \\ (R^{\mathrm{II}}) \end{bmatrix} \tag{10}$$

where the submatrices are already described in [13].

The modal scattering matrix of the double plane step discontinuity of the rectangular waveguides of different cross section, regions 0 to I (Fig. 1(c)), is already derived in [25]. The series of step discontinuities for a complete filter structure is calculated by direct combination of the single modal scattering matrices, and the corresponding relations are given in [13], [24], and [25]. As with metal insert filters and finned transformers [13], [24], the computer-aided design is carried out by an optimization program applying the evolution strategy method. An error function is minimized with respect to a parameter vector which contains the coupling and resonator lengths as well as the slot widths (Fig. 1(c)).

III. Results

Fig. 3 shows the calculated transmission coefficient $|S_{21}|$ in dB as a function of frequency of a quasi-high-pass filter where the gap width $w/b = 0.81$ is relatively high. A WR 90 (22.86 mm × 10.16 mm) waveguide housing is chosen for the input and output waveguide, and the ridge waveguide section utilizes a WR 42 (10.668 mm × 4.318 mm) waveguide housing. In Fig. 3(a), the transverse resonance method (TRM) is used to solve the related ridge waveguide eigenvalue problem and parts (b) and (c) of the figure show the solutions with the standing wave formulation (SWF) and the resonator method (RM), respectively. Seven TM modes and 12 TE modes in (2) and (3), together with $M = N = 9$ expansion terms in (4)–(8), have been used. Good agreement between the results of the three different mode-matching techniques is given.

In order to check the three different cross-section formulations of the ridge waveguide against experimental data, Fig. 4(a) shows the calculated and measured input reflection coefficient $|S_{11}|$ in dB as a function of frequency of a very simple, nonoptimized filter structure with four bilateral E-plane fins in a single WR-62 waveguide (15.799 mm × 7.899 mm) housing (cf. Fig. 4(b)). The thickness of the fins is $t = 0.9$ mm, and the gap width $w/b = 0.39$ is about half that of the preceding case (Fig. 3). Due to the smaller gap width, the three different mode-matching techniques applied—TRM (solid line), SWF (dashed line), RM (dash–dotted line)—lead to different solutions. This is particularly true for the RM. The numbers of modes and expansion terms are equivalent to those chosen for calculating the results in Fig. 3. The mechanical tolerances of the structure (which have been measured by a measuring microscope) are taken into account in the analysis; for the slightly oblique gaps, a mean value for the corresponding gap width has been assumed. Very

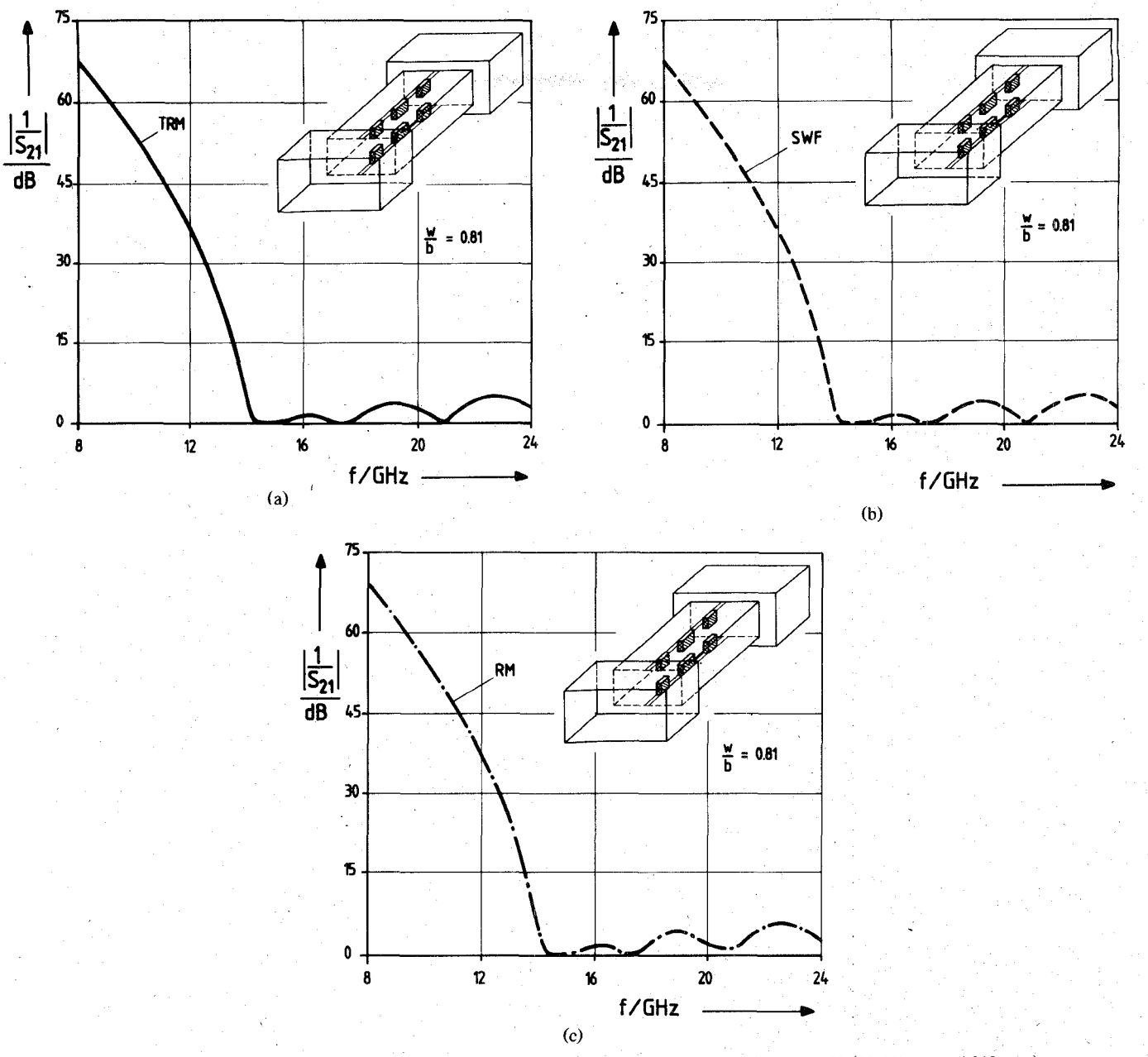

Fig. 3. Quasi-high-pass filter. WR 90 (22.86 mm×10.16 mm) input/output waveguide, WR 42 (10.668 mm×4.318 mm) ridge waveguide section. Filter dimensions (cf. Fig. 1): $t = 1$ mm, $l_{C1} = l_{C4} = 0.236$ mm, $l_{R1} = l_{R3} = 1.001$ mm, $l_{C2} = l_{C3} = 11.429$ mm, $l_{R2} = 1.58$ mm. (a) Transverse resonance method (TRM) solution of the eigenvalue problem. (b) Standing wave formulation (SWF) solution of the eigenvalue problem. (c) Resonator method (RM) solution of the eigenvalue problem.

good agreement between theory and measurements has been achieved for the TRM.

For still smaller gap widths, $w/b = 0.116$, the difference between the results obtained by applying the TRM (solid line) and, particularly, the RM (dash–dotted line) is increased further. Fig. 5 shows the calculated transmission coefficient $|S_{21}|$ for an optimized X-band evanescent-mode E-plane finned waveguide band-pass filter design example with passband at about 12 GHz. As in Fig. 3, a WR 90 waveguide housing is chosen for the input/output waveguide and a WR 42 housing for the filter section. Seven TE modes and 12 TM modes are utilized in (2) and (3); the numbers of expansion terms chosen were $N = 5$ for the TRM and $M = 4$ and $N = 9$ for the SWF and the RM respectively. In order to search the cutoff frequencies for the related ridge waveguide cross-section eigenvalue problem, the frequency step widths in the numerical search algorithm for the SWF and the RM have been set to 1% of the corresponding step width utilized in the search algorithm for the TRM. In spite of the large increase in CPU time (approximately a factor of 4 for a complete frequency response calculation), important modes in the eigenvalue solution formulated by the SWF, and particularly by the RM, have been overlooked. For small gap widths, therefore, both the SWF and particularly the RM are considered to be inap-

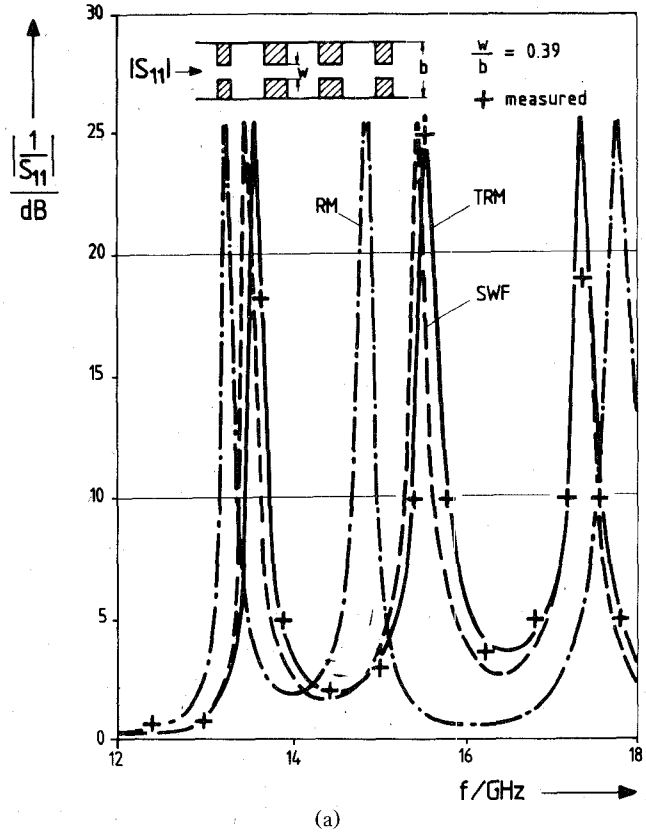

(a)

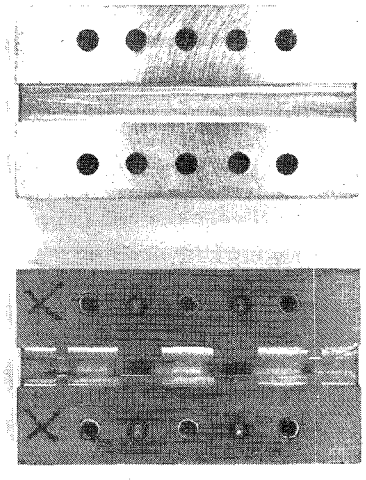

(b)

Fig. 4. Nonoptimized simple filter structure, to verify the theory. Four bilateral E-plane fins in a single WR 62 waveguide housing; measured dimensions: 15.85 mm×7.925 mm, fin thickness $t = 0.9$ mm, gap width $w = 3.1$ mm. Filter dimensions (cf. Fig. 1): $l_{C2} = l_{C4} = 1.025$ mm, $l_{R1} = l_{R4} = 2.6$ mm, $l_{C3} = 10.5$ mm, $l_{R2} = l_{R3} = 8.95$ mm. (a) Calculated and measured (+) input reflection coefficient $|S_{11}|$ in decibels versus frequency. Transverse resonance method (TRM, solid line), standing wave formulation (SWF, dashed line), and resonator method (RM, dash–dotted line). (b) Photograph of the realized structure.

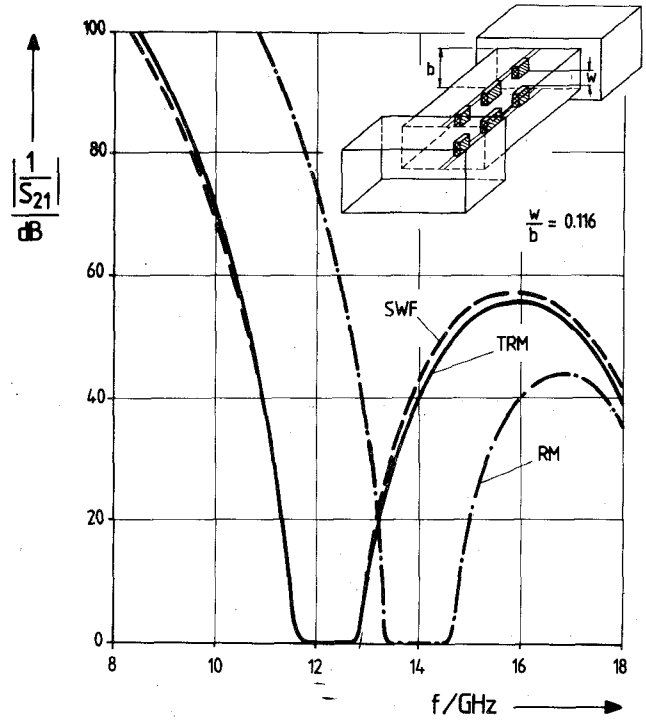

Fig. 5. Computer-optimized X-band evanescent-mode E-plane finned waveguide band-pass filter. WR 90 (22.86 mm×10.16 mm) waveguide input and output housing; WR 42, (10.668 mm×4.318 mm) below-cutoff waveguide. Fin thickness $t = 1$ mm; gap width $w = 0.5$ mm. Design with five E-plane fins. $l_{C1} = l_{C6} = 0.2$ mm; $l_{R1} = l_{R5} = 0.975$ mm, $l_{C2} = l_{C5} = 10.944$ mm, $l_{R2} = l_{R4} = 1.541$ mm, $l_{C3} = l_{C4} = 12.120$ mm, $l_{R3} = 1.491$ mm; 12 TE, 7 TM modes. Expansion terms: $N = 5$ (TRM), $N = 9$, $M = 4$ (SWF, RM). Transmission coefficient applying the transverse resonance method (TRM, solid line), the standing wave formulation (SWF, dashed line), and the resonator method (RM, dash–dotted line) for the related eigenvalue solution.

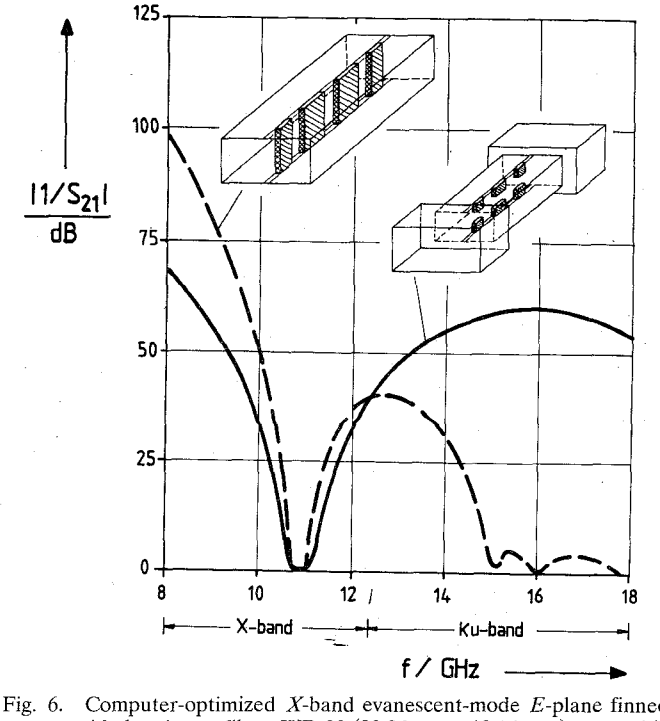

Fig. 6. Computer-optimized X-band evanescent-mode E-plane finned waveguide band-pass filter. WR 90 (22.86 mm×10.16 mm) waveguide input and output housing; WR 42 (10.668 mm×4.318 mm) below-cutoff waveguide. Fin thickness $t = 1$ mm; gap width $w = 0.975$ mm.

propriate for adequately solving the related eigenvalue problem. The final computer-optimized design, therefore, is carried out by utilizing the TRM.

An optimized X-band evanescent-mode E-plane finned waveguide band-pass filter design example with passband

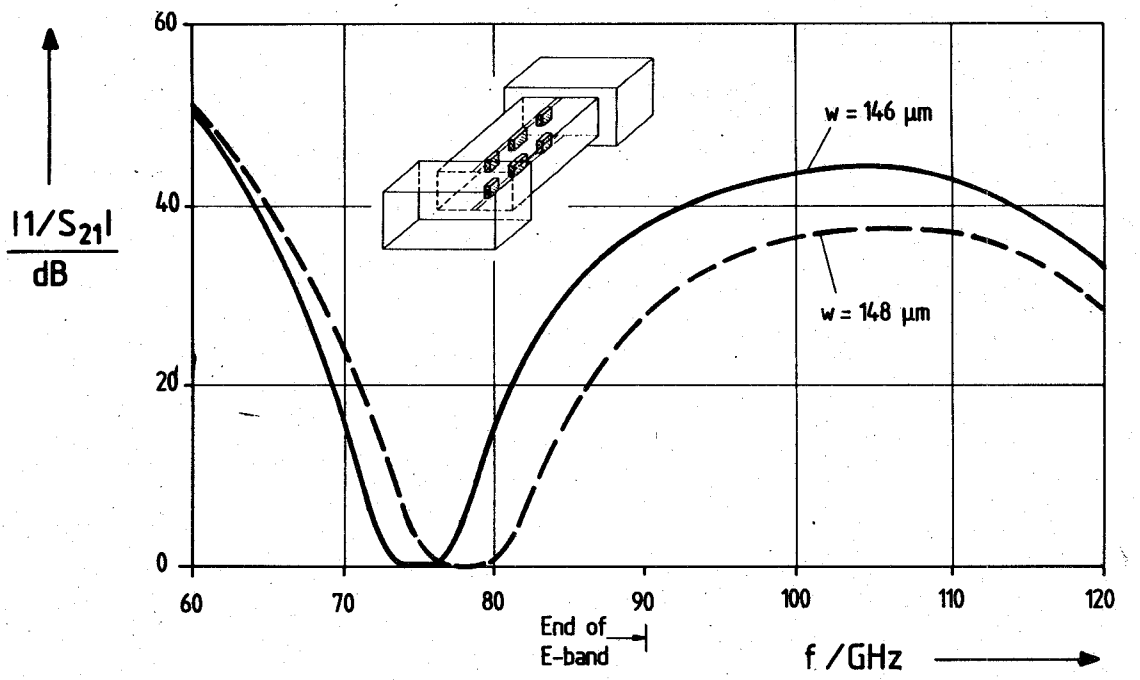

Fig. 7. Computer-optimized E-band evanescent-mode E-plane finned waveguide band-pass filter. WR 12 (3.098 mm × 1.549 mm) input and output waveguide; WR 7 below-cutoff waveguide which is reduced in height ($a = 1.651$ mm, $b = 0.668$ mm). Fin thickness $t = 150$ μm; gap width $w = 0.146$ μm.

at about 11 GHz is shown in Fig. 6. The design with three E-plane fins of thickness $t = 1$ mm, a WR 90 input and output waveguide, and a WR 42 below-cutoff waveguide achieves an attenuation in the second stopband of more than 50 dB above 13.5 GHz and within the adjacent Ku-band. A comparison with the characteristic of a corresponding E-plane metal-insert coupled resonator filter [24] with three resonators (dashed line) demonstrates the significant improvement in rejection given by the E-plane printed-circuit evanescent-mode filter technique.

Fig. 7 shows the results of a computer-optimized E-band evanescent-mode E-plane finned waveguide band-pass filter design example with a WR 12 (3.098 mm × 1.549 mm) input and output waveguide and with a WR 7 waveguide reduced in height (1.651 mm × 0.668 mm) for the below-cutoff filter section. This design, with three E-plane fins of thickness $t = 150$ μm, achieves a minimum stopband attenuation of more than 40 dB up to about 110 GHz (the end of the next higher frequency band, the W-band). The sensitivity of the performance of the optimized E-band filter to dimensional tolerances is demonstrated by the dashed curve, which shows the insertion loss for a fin gap width increased by only 2 μm.

Fig. 8 presents a comparison between theoretical and measured data for the structure currently under investigation. An easily fabricated Ku-band three-resonator evanescent-mode E-plane finned waveguide filter (Fig. 8(b)) with a fin thickness of $t = 1$ mm has been realized by a simple milling technique. A WR 90 waveguide housing has been chosen for the input/output waveguide, and the filter section is a WR 42 waveguide below cutoff. The measured insertion loss over the passband is only about 0.2 dB. Good agreement between measurements and theory is given (cf. Fig. 8(a)) if the actual geometrical dimensions of the filter (measured by a measuring microscope) are taken into account in the calculations. This holds also for the return loss curve which has significantly higher sensitivity to design tolerances. As a consequence, these results demonstrate the validity of the proposed design technique in the practical realization of these filters. The filter characteristics of Figs. 7 and 8(a) not only illustrate the necessity for a reliable design theory taking into account all relevant parameters but also show the requirement for high-precision fabrication facilities.

IV. Conclusion

The modal S-matrix method presented here achieves an exact computer-aided design of compact, low-cost, low-insertion-loss evanescent-mode bilateral E-plane finned waveguide band-pass filters with wide stopbands. The theory, which includes the finite thickness of the fins as well as higher order mode interactions at all discontinuities, leads to a reliable prediction of the filter characteristic and allows the stopband characteristic of the filter to be taken into account in the optimization process. Moreover, this design leads to relatively wide gap widths, which may help to meet high power handling requirements. The numerical advantage of the transverse resonance method for solving the related cross-sectional eigenvalue problem of the ridge waveguide section is demonstrated by comparison with solutions obtained by the more classical standing wave or resonator mode-matching techniques. The theory shows excellent agreement with the measurements presented.

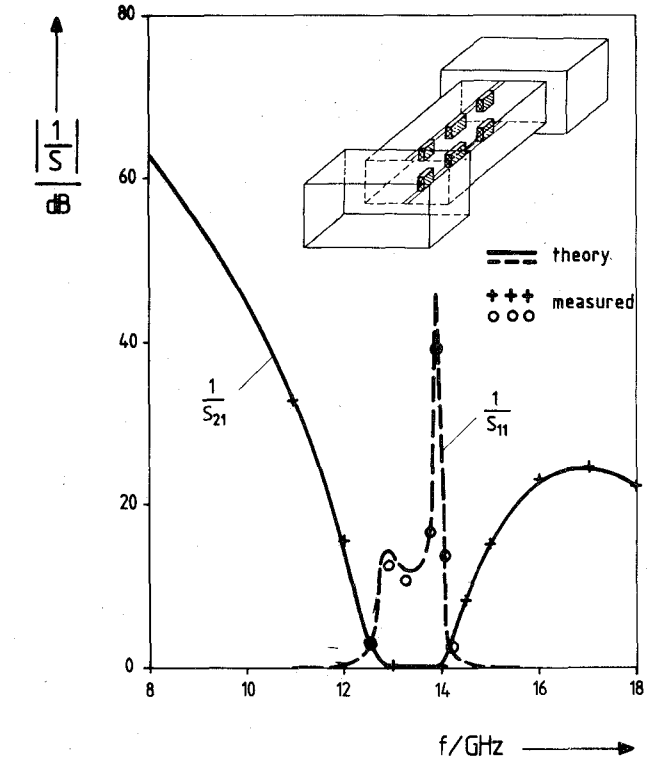

(a)

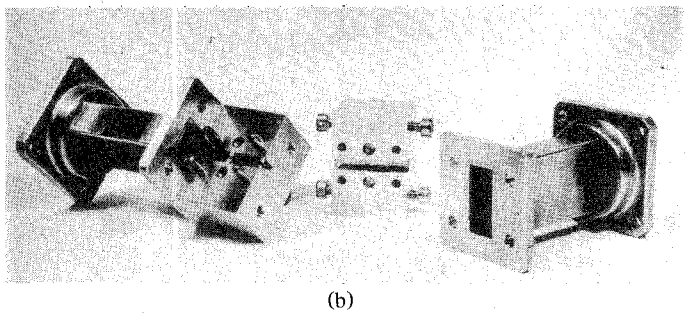

(b)

Fig. 8. *Ku*-band three-resonator evanescent-mode *E*-plane finned waveguide filter with a fin thickness of $t = 1$ mm realized by a simple filing technique. WR 90 input/output waveguide, WR 42 waveguide below-cutoff filter section. Actual dimensions: $a_1 \times b_1 = 22.85$ mm $\times$ 10.15 mm; $a \times b = 10.66$ mm $\times$ 4.29 mm; $t = 1$ mm, $l_{c1} = 0.25$ mm, $l_{c2} = l_{c3} = 11.45$ mm, $l_{c4} = 0.24$ mm, $l_{R1} = 0.99$ mm, $l_{R2} = 1.6$ mm, $l_{R3} = 1.01$ mm; $w_1 = w_2 = w_3 = 0.98$ mm. Number of expansion terms used $N = 9$ (cf. eq. (6)); modal scattering matrix calculated with 20 TE and 12 TM modes. (a) Calculated (——) and measured (+) filter response. (b) Photograph of the prototype under investigation.

Appendix
Abbreviations for the Cross-Section Eigenfunction in (8)

$$F^{\mathrm{IIa}}_{xHqm} = \frac{\sin\left\{k^{\mathrm{IIa}}_{zHqm}\left(x-\frac{a}{2}\right)\right\}}{k^{\mathrm{IIa}}_{zHqm}} - \frac{\cos\left\{k^{\mathrm{IIa}}_{xHqm}\left(\frac{a}{2}-e\right)\right\}}{k^{\mathrm{IIa}}_{xHqm}\sin\left(k^{\mathrm{IIa}}_{xHqm}e\right)}\cos\left(k^{\mathrm{IIa}}_{xHqm}x\right) \quad \text{(A1)}$$

$$F^{\mathrm{IIb}}_{yHqn} = \cos\left(k^{\mathrm{IIb}}_{yHqn}y\right) - \frac{\sin\left(k^{\mathrm{IIb}}_{yHqn}c\right)}{\sin\left\{k^{\mathrm{IIb}}_{yHqn}\left(\frac{b}{2}-c\right)\right\}}\cos\left\{k^{\mathrm{IIb}}_{yHqn}\left(y-\frac{b}{2}\right)\right\} \quad \text{(A2)}$$

$$F^{\mathrm{IIa}}_{xEpm} = \cos\left\{k^{\mathrm{IIa}}_{xEpm}\left(x-\frac{a}{2}\right)\right\} + \frac{\cos\left\{k^{\mathrm{IIa}}_{xEpm}\left(\frac{a}{2}-e\right)\right\}}{\sin\left(k^{\mathrm{IIa}}_{xEpm}e\right)}\sin\left(k^{\mathrm{IIa}}_{xEpm}x\right) \quad \text{(A3)}$$

$$F^{\mathrm{IIb}}_{yEpn} = \frac{\sin\left(k^{\mathrm{IIb}}_{yEpn}y\right)}{k^{\mathrm{IIb}}_{yEpn}} - \frac{\sin\left(k^{\mathrm{IIb}}_{yEpn}c\right)}{k^{\mathrm{IIb}}_{yEpn}\sin\left\{k^{\mathrm{IIb}}_{yEpn}\left(\frac{b}{2}-c\right)\right\}}\sin\left\{k^{\mathrm{IIb}}_{yEpn}\left(y-\frac{b}{2}\right)\right\}. \quad \text{(A4)}$$

References

[1] S. B. Cohn, "Optimum design of stepped transmission-line transformers," *IRE Trans. Microwave Theory Tech.*, vol. MTT-3, pp. 16–21, Apr. 1955.

[2] S. Hopfer, "The design of ridged waveguide," *IRE Trans. Microwave Theory Tech.*, vol. MTT-3, pp. 20–29, Oct. 1955.

[3] E. S. Hensperger, "Broad-band stepped transformers from rectangular to double-ridged waveguide," *IRE Trans. Microwave Theory Tech.*, vol. MTT-6, pp. 311–314, July 1955.

[4] J. P. Montgomery, "On the complete eigenvalue solution of ridged waveguide," *IEEE Trans. Microwave Theory Tech.*, vol. MTT-19, pp. 547–555, June 1971.

[5] W. J. R. Hoefer and M. N. Burtin, "Closed-form expressions for the parameters of finned and ridged waveguides," *IEEE Trans. Microwave Theory Tech.*, vol. MTT-30, pp. 2190–2194, Dec. 1982.

[6] Y. Utsumi, "Variational analysis of ridged waveguide modes," *IEEE Trans. Microwave Theory Tech.*, vol. MTT-33, pp. 111–120, Feb. 1985.

[7] Y. Konishi and H. Matsumura, "Short end effect of ridge guide with planar circuit mounted in a waveguide," *IEEE Trans. Microwave Theory Tech.*, vol. MTT-27, pp. 168–170, Feb. 1979.

[8] D. Mirshekar-Syahkal and J. B. Davies, "Accurate analysis of tapered planar transmission lines for microwave integrated circuits," *IEEE Trans. Microwave Theory Tech.*, vol. MTT-29, pp. 123–128, Feb. 1981.

[9] L.-P. Schmidt and H. Meinel, "Broadband millimeter-wave PIN-diode attenuator with double-ridged waveguide flanges," *Electron. Lett.*, vol. 18, no. 19, pp. 839–840, Sept. 1982.

[10] P. J. Meier, "Integrated finline: The second decade," *Microwave J.*, vol. 28, no. 11, pp. 31–54, Nov. 1985; also no. 12, pp. 30–48, Dec. 1985.

[11] A. M. K. Saad, "Novel lowpass harmonic filters for satellite application," in *IEEE MTT-S Int. Microwave Symp. Dig.*, 1984, pp. 292–294.

[12] Q. Zhang and T. Itoh, "Computer-aided design of evanescent-mode waveguide filter with non-touching *E*-plane fins," *IEEE Trans. Microwave Theory Tech.*, vol. 36, pp. 404–412, Feb. 1988.

[13] J. Bornemann and F. Arndt, "Modal-*S*-matrix design of optimum stepped ridged and finned waveguide transformers," *IEEE Trans. Microwave Theory Tech.*, vol. MTT-35, pp. 561–567, June 1987.

[14] R. R. Mansour, R. S. K. Tong, and R. H. McPhie, "Simplified description of the field distribution in finlines and ridge waveguides and its application to the analysis of *E*-plane discontinuities," *IEEE Trans. Microwave Theory Tech.*, vol. 36, pp. 1825–1832, Dec. 1988.

[15] H. F. Chappell, "Waveguide low pass filter using evanescent mode inductors," *Microwave J.*, vol. 21, pp. 71–72, Dec. 1978.

[16] G. Graven and C. K. Mok, "The design of evanescent mode waveguide band-pass filters for a prescribed insertion loss characteristic," *IEEE Trans. Microwave Theory Tech.*, vol. MTT-19, pp. 295–308, 1971.
[17] R. V. Snyder, "New application of evanescent mode waveguide to filter design," *IEEE Trans. Microwave Theory Tech.*, vol. MTT-25, pp. 1013–1021, Dec. 1977.
[18] R. V. Snyder, "Broadband waveguide or coaxial filters with wide stopbands, using a stepped-wall evanescent mode approach," *Microwave J.*, vol. 26, pp. 53–58, Dec. 1983.
[19] F. Arndt and G. U. Paul, "The reflection definition of the characteristic impedance of microstrips," *IEEE Trans. Microwave Theory Tech.*, vol. MTT-27, pp. 724–731, Aug. 1979.
[20] R. Vahldieck and J. Bornemann, "A modified mode-matching technique and its application to a class of quasi-planar transmission-lines," *IEEE Trans. Microwave Theory Tech.*, vol. MTT-33, pp. 916–926, Oct. 1985.
[21] R. Sorrentino and T. Itoh, "Transverse resonance analysis of fin-line discontinuities," *IEEE Trans. Microwave Theory Tech.*, vol. MTT-32, pp. 1633–1638, Dec. 1984.
[22] A. Wexler, "Solution of waveguide discontinuities by modal analysis," *IEEE Trans. Microwave Theory Tech.*, vol. MTT-15, pp. 508–517, Sept. 1967.
[23] E. Kühn, "A mode-matching method for solving field problems in waveguide and resonator circuits," *Arch. Elek. Übertragung.*, vol. 27, pp. 511–518, Dec. 1973.
[24] R. Vahldieck, J. Bornemann, F. Arndt, and D. Grauerholz, "Optimized waveguide *E*-plane metal insert filters for millimeter-wave applications," *IEEE Trans. Microwave Theory Tech.*, vol. MTT-31, pp. 65–69, Jan. 1983.
[25] H. Patzelt and F. Arndt, "Double-plane steps in rectangular waveguides and their application for transformers, irises, and filters," *IEEE Trans. Microwave Theory Tech.*, vol. MTT-30, pp. 771–776, May 1982.

✠

Jens Bornemann (M'87) was born in Hamburg, West Germany, on May 26, 1952. He received the Dipl.-Ing. and Dr.-Ing. degrees, both in electrical engineering, from the University of Bremen, West Germany, in 1980 and 1984, respectively.

From 1980 to 1983, he was a Research and Teaching Assistant in the Microwave Department at the University of Bremen, working on quasi-planar waveguide configurations and computer-aided *E*-plane filter design. After a two-year period as a consulting engineer, he joined the University of Bremen again, in 1985, as an Assistant Professor. Since April 1988, he has been an Associate Professor at the University of Victoria, Victoria, B.C., Canada. His current research activities include microwave system design, active components, and problems of electromagnetic field theory.

Dr. Bornemann was one of the recipients of the A. F. Bulgin Premium of the Institution of Electronic and Radio Engineers in 1983. He

✠

Fritz Arndt (SM'83) received the Dipl. Ing., Dr. Ing., and Habilitation degrees from the Technical University of Darmstadt, Germany, in 1963, 1968, and 1972, respectively.

From 1963 to 1973, he worked on directional couplers and microstrip techniques at the Technical University of Darmstadt. Since 1972, he has been a Professor and Head of the Microwave Department of the University of Bremen, Germany. His research activities center on field problems of waveguide, finline, and optical waveguide structures, antenna design, and scattering structures.

Dr. Arndt is a member of the VDE and NTG (Germany). He received the NTG award in 1970, the A. F. Bulgin Award (together with three coauthors) from the Institution of Radio and Electronic Engineers in 1983, and the best paper award of the antenna conference JINA 1986 (France).